Kinematics-based Adaptive Assistance of a Semi-Passive Upper-Limb Exoskeleton for Workers in Static and Dynamic Tasks

Lorenzo Grazi[1], *Member, IEEE*, Emilio Trigili[1], *Member, IEEE*, Noemi Caloi[2], Giulia Ramella[1], Francesco Giovacchini[3], Nicola Vitiello*[1,4], *Member, IEEE*, and Simona Crea*[1,4], *Member, IEEE*

***Abstract*— Typical industrial work activities may include a variety of different gestures, entailing the execution of dynamic and static movements. Occupational upper-limb exoskeletons can assist the shoulder complex in both static and dynamic gestures, but the required assistance level may be different according to the tasks. This article presents the design, development, and experimental evaluation of a novel kinematics-based adaptive assistance algorithm for a semi-passive upper-limb exoskeleton. The algorithm uses kinematic signals gathered by onboard sensors to set the assistance amplitude according to the type of movement being executed. Experimental activities were performed to assess the algorithm's performance. Results show that the algorithm can effectively provide different assistance levels according to the type of task being executed, such as the minimum level for more dynamic tasks and the maximum level for the most static activities. Additionally, compared to working without the exoskeleton, the exoskeleton controlled by the proposed adaptive algorithm can reduce the users' flexor muscular activity in both dynamic and static tasks, respectively by 24 ± 6% and 42 ± 2%. Similar results were reported for extensor muscles, which reduced their activations by 7 ± 3%, and 40 ± 4% in dynamic and static tasks.**

***Index Terms*— Adaptive control, upper-limb exoskeletons, wearable robotics, workers assistance**

Manuscript received: February 24, 2022; Revised: April 29, 2022; Accepted: June 18, 2022.

This paper was recommended for publication by Editor Jee-Hwan Ryu upon evaluation of the Associate Editor and Reviewers' comments.

This work has been supported by the EU within the Mari4_YARD project (H2020-MG-2020-SingleStage-INEA) under Grant Agreement: 101006798.
Corresponding author: Lorenzo Grazi (lorenzo.grazi@santannapisa.it)

[1]L. Grazi, E. Trigili, G. Ramella, N. Vitiello, and S. Crea are with The BioRobotics Institute, Scuola Superiore Sant'Anna, Pontedera, Pisa, Italy, and also with the Department of Excellence in Robotics & AI, Pisa, Italy (emilio.trigili@santannapisa.it, giulia.ramella@santannapisa.it, nicola.vitiello@santannapisa.it, simona.crea@santannapisa.it).

[2]N. Caloi was with the BioRobotics Institute, Scuola Superiore Sant'Anna, Pontedera, Pisa, Italy when the activities described in this paper were carried out (noemi.caloi@outlook.com)

[3]F. Giovacchini is with IUVO S.r.l., Pontedera, Pisa, Italy (francesco.giovacchini@iuvo.company).

[4]N. Vitiello and S. Crea are also with IRCCS Fondazione Don Carlo Gnocchi (Florence, Italy).

*N. Vitiello and S. Crea share the senior authorship.

F. Giovacchini, N. Vitiello, and S. Crea are shareholders and thus have commercial interests in IUVO S.r.l., a spin-off company of Scuola Superiore Sant'Anna, which designed the technology described in this paper. IUVO S.r.l. is the owner of the IP protecting the H-PULSE technology.

This work involved human subjects in its research. Approval of all ethical and experimental procedures and protocols was granted by the Joint Ethics Committee of Scuola Superiore Sant'Anna and Scuola Normale Superiore under approval n. 2/2019 and performed in line with the Declaration of Helsinki.

Digital Object Identifier (DOI): see top of this page.

I. Introduction

Intensive overhead and repetitive manual works are among the main risk factors for developing shoulder work-related musculoskeletal disorders (WMSDs), such as shoulder impingement syndrome and rotator cuff tendinopathies [1]. To complement common preventive measures implemented in industrial settings to reduce the occurrence of WMSDs, upper-limb exoskeletons are emerging as a promising intervention to reduce the biomechanical load on specific human joints [2].

Exoskeletons can be classified into passive and active systems; passive devices usually rely on elastic elements to store and release energy and to provide the user with antigravitational support, while active systems require sensors and control units to generate the assistive torque through powered actuators [3], [4]. Active systems can generate versatile torque profiles according to the performed task, but they are usually heavier and bulkier than their passive counterparts, hence resulting in lower usability in operational scenarios [5], [6]. Passive exoskeletons have been tested both in laboratory and field studies extensively, with results showing in most cases reduced muscular strain and perceived fatigue [7]–[12]. However, some studies showed higher activations of the antagonistic muscles when moving against the assistance (specifically while lowering the arms) [6], [13]. Very recently, new types of exoskeletons have been proposed, such as hybrid active-passive exoskeletons, combining passive and active solutions at different joints [14], and semi-passive exoskeletons, designed to adapt the passive behavior of the system, e.g., by automatically adapting the level of assistance or engaging/disengaging the actuation mechanisms through active clutches, according to the task, the user's stress level, or other context-related factors [3].

This paper presents a novel adaptive algorithm aimed at automatically setting the level of assistance, based on kinematic information extracted from joint angle sensors integrated into a semi-passive shoulder exoskeleton, named H-PULSE. The mechatronics of the device has been presented in a previous work [15]. Along with the description of the

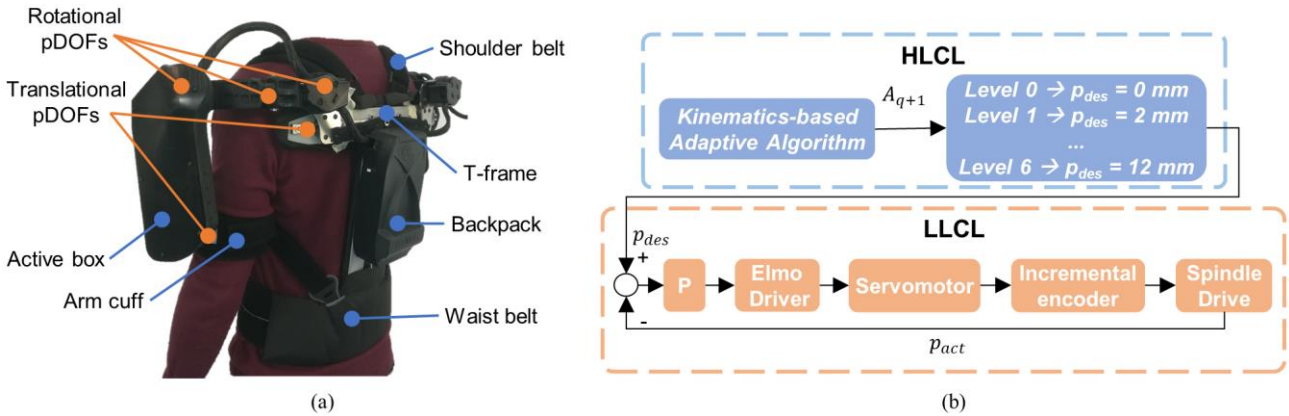

Fig. 1 (a) The H-PULSE exoskeleton. Blue lines indicate main exoskeleton's modules; orange lines indicate locations of the pDOFs. (b) Block diagram of the two-layer control architecture of the H-PULSE, made of high-level control layer (HLCL) and low-level-control layer (LLCL).

algorithm, this paper presents experiments with healthy subjects for the evaluation of the performance of the algorithm

II. H-PULSE EXOSKELETON

H-PULSE is a semi-passive upper-limb exoskeleton for workers' assistance in manual work activities [Fig. 1(a)][15]. It was designed by IUVO S.r.l. (Pontedera, Pisa, Italy) and the technology is patented [16]. The exoskeleton weighs 5 kg and integrates four main modules: (i) a garment as a physical Human-Robot Interface (pHRI), (ii) a chain of passive degrees of freedom (pDOFs), (iii) two actuation boxes with a spring-loaded mechanism generating the assistive torque and a servomotor to set the level of the springs pre-tension, and (iv) the control unit.

The pHRI is made of a T-shaped aluminum alloy frame, and adjustable pelvis and shoulder belts to ensure a fast and easy wearing procedure, while C-shaped cuffs connect the user's arms to the actuation boxes. The pHRI ensures the comfort of the user and the transfer of the exoskeleton's weight to the pelvis. The chain of pDOFs includes five DOFs (two translational and three rotational), designed in such a way to comply with the physiological range of motion (RoM) of the glenohumeral joint and to transfer the counteractive forces generated by the active boxes to the pelvis while assisting the shoulder flexion/extension (sFE). Each active box contains a spring-based mechanism to generate the assistive torque around the sFE joint. The assistive torque profile is hard-coded in the spring-based mechanism, and it is designed to partially compensate for the gravitational torque of the human arm. A low-power tuning mechanism, made of a spindle drive coupled with a servomotor driven by a control unit, allows to automatically change the pre-tensioning of the springs (maximum springs displacement is 12 mm) and, consequently, the assistive level. In this work, two consecutive levels are separated by 2 mm of spring displacement, resulting in 7 possible assistive levels, ranging from about 4.5 to 6 N·m; considering that about 1 N·m is needed to compensate for the weight of the active box, the net torque range for the user's arm gravity compensation is sufficient to provide at least the 20% of the arm gravitational torque of the 5 – 95% of males population, whose maximum shoulder torques range between about 10 to 23 N·m [17].

and its efficacy on muscle activities across different types of static and dynamic work tasks.

A backpack placed in the rear part of the pHRI houses the electronics and batteries to operate the exoskeleton. The control system is made of a two-layer hierarchical architecture, comprising low-level and high-level control layers, running on a NI System-on-Module (National Instruments, Austin, TX, USA) [Fig. 1(b)]. The low-level control layer (LLCL) runs on a field-programmable gate array processor (Zynq-7020, Xilinx, San José, CA, USA). It is used for reading the joint sensors and driving the servomotors via a position control on the motor's incremental encoder. About 5 seconds are needed to vary the pre-tensioning of the spring by 2 mm, i.e., for completing a one-level change of assistance. The high-level control layer (HLCL) runs on a dual-core real-time ARM controller and runs the kinematics-based adaptive assistive algorithm that sets the desired assistive level.

III. KINEMATICS-BASED ADAPTIVE ALGORITHM

A. *Hypotheses and Goal*

The objective of the presented algorithm is to provide the H-PULSE with the capability to adaptively set an appropriate level of assistance based on the observed movement kinematics, without requiring a priori knowledge or real-time classification of the task.

To design the adaptive algorithm, two main considerations were made. First, movement kinematics can be seen as the combined contribution of low- and high-frequency components, namely as the combination of static and dynamic movements. Second, we assumed that the exoskeleton assistance should increase with the degree of the static nature of the movement, to support the force exerted by the arm flexors and abductors that mainly contribute to keeping the arms raised, by counterbalancing the arms' gravitational torque at the glenohumeral joint; also, we considered that the assistance level should decrease as the dynamic characteristics of the movement increase, to support the eccentric work done by the flexor muscles during arms extension and at the same time preventing the action of the antagonistic (extensor) muscles against the device assistance [13], [18], [19].

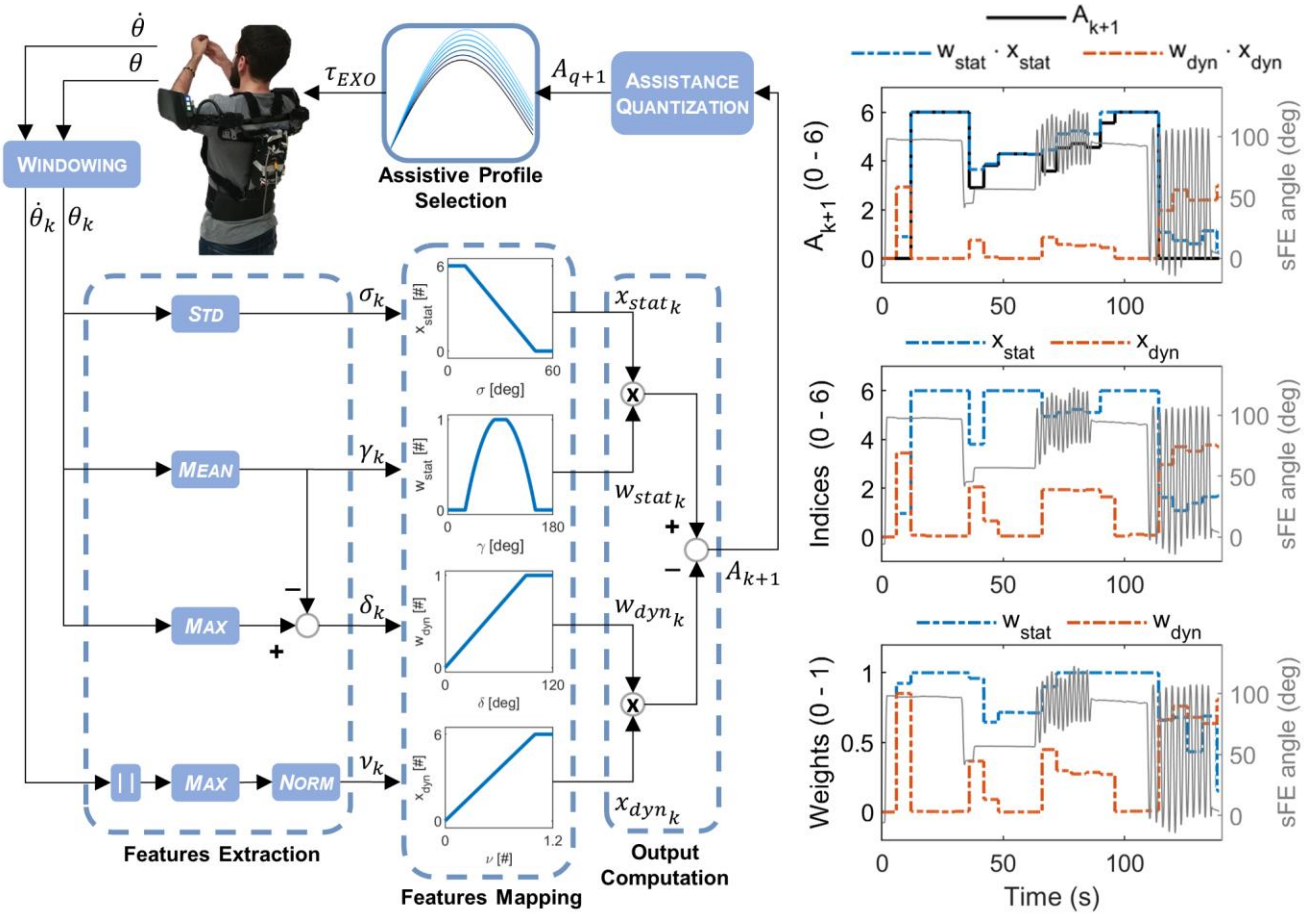

(a) (b)

Fig. 2 (a) Block diagram of the kinematics-based adaptive assistance algorithm running on the high-level control layer of the H-PULSE exoskeleton. (b) Algorithm's output, indices, and weights computed from an exemplary dataset including a sequence of static and dynamic movements, performed at different shoulder elevation angle and velocity.

B. *Kinematics-based Adaptive Algorithm*

The proposed kinematics-based adaptive algorithm is composed of four main steps [Fig. 2(a)]: i) input signal windowing, ii) features extraction, iii) features mapping through membership functions, and iv) output computation.

Input signal windowing. In this step, the sFE angle (θ) and velocity ($\dot{\theta}$, computed by real-time differentiation of θ through the 2nd-order central method) are collected into a 6-seconds non-overlapping virtual buffer. The length of the buffer was chosen slightly greater than the time needed to make a single assistance level change (i.e., 5 seconds).

Features extraction. Four features are extracted from the signals collected in the buffer every 6 seconds. From the sFE angle vector (θ_k) the algorithm extracts: the mean angle (γ_k), the angle standard deviation (σ_k), and the maximum displacement from the mean (δ_k) computed as in Eq. (1):

$$\delta_k = max(\theta_k) - \gamma_k \tag{1}$$

where θ_k can range between 0 and 180 deg.

The sFE velocity vector $\dot{\theta}_k$ is used to compute the normalized maximum velocity, according to Eq. (2):

$$\nu_k = max(|\dot{\theta}_k|)/\omega \tag{2}$$

where ω = 360 deg/s is the maximum joint angle velocity, empirically defined for this application.

Features mapping. Once the features are extracted, they are mapped through membership functions into static and dynamic indices (x) and weights (w) (Table I).

TABLE I Features mapping to compute algorithm's indices and weights.

Feature	Index/weight
σ_k	$x_{stat_k} = \begin{cases} 6, & \sigma_k \le \sigma^m \\ 0, & \sigma_k \ge \sigma^M \\ 6\dfrac{(\sigma_k^M - \sigma_k)}{(\sigma_k^M - \sigma_k^m)}, & \sigma^m < \sigma_k < \sigma^M \end{cases}$
γ_k	$w_{stat_k} = \begin{cases} 0, & (\gamma_k \le \gamma^m) \wedge (\gamma_k \ge \gamma^M) \\ 1, & \gamma_{sat}^m \le \gamma_k \le \gamma_{sat}^M \\ a{\gamma_k}^2 + b\gamma_k + c, & (\gamma^m < \gamma_k < \gamma_{sat}^m) \wedge (\gamma_{sat}^M < \gamma_k < \gamma^M) \end{cases}$
δ_k	$w_{dyn_k} = \begin{cases} \delta_k, & \delta_k \le \delta^{max} \\ 1, & \delta_k > \delta^{max} \end{cases}$
ν_k	$x_{dyn_k} = \begin{cases} \nu_k, & \nu_k \le \nu^M \\ 6, & \nu_k > \nu^M \end{cases}$

$\sigma^m = 10\ deg,\ \sigma^M = 50\ deg,\ \gamma^m = 30\ deg,\ \gamma^M = 150\ deg,$ $\gamma_{sat}^m = 80\ deg,\ \gamma_{sat}^M = 100\ deg,\ \delta^M = 90\ deg,\ \nu^M = 1$ are threshold values. a, b, c are parabola parameters.

The static index (x_{stat_k}) is modelled as an inversely linear function of σ_k for $10 \leq \sigma_k \leq 50$ deg; instead, the dynamic index (x_{dyn_k}) is modelled as a linear function of ν_k for $0 \leq \nu_k \leq 1$. Both indices can range continuously between 0 and 6, representing the range of assistance levels.

The static weight (w_{stat_k}) is modelled as a modified parabolic function of γ_k, centered around 90 deg, resembling the gravity torque on the sFE joint; this function is null for $\gamma_k \leq 30$ deg and $\gamma_k \geq 150$ deg, and maximum for $80 \leq \gamma_k \leq 100$ deg. The dynamic weight (w_{dyn_k}) is modelled as a linear function of δ_k for $0 \leq \delta_k \leq 90$ deg. Both weights can range continuously between 0 and 1.

Threshold values used to compute indices and weights were chosen empirically by looking at pilot data.

Output computation. The output of the algorithm (A_{k+1}), computed at the k-th window, is defined according to Eq. (3):

$$A_{k+1} = A_{stat_k}(\gamma_k, \sigma_k) - A_{dyn_k}(\delta_k, \nu_k) \tag{3}$$

where $A_{stat_k}(\gamma_k, \sigma_k) = w_{stat_k}(\gamma_k) \cdot x_{stat_k}(\sigma_k)$ and $A_{dyn_k}(\delta_k, \nu_k) = w_{dyn_k}(\delta_k) \cdot x_{dyn_k}(\nu_k)$ are the static and dynamic contributions to A_{k+1}, respectively.

Finally, A_{k+1} value is quantized to generate a discrete assistance level (A_{q+1}). The corresponding spindle drive position is then commanded to the LLCL. An example of the algorithm's output, indices, and weights during an exemplary trial is shown in Fig. 2(b).

IV. Experimental Evaluation

Two experimental sessions were carried out to (i) characterize the algorithm's output and (ii) verify the effectiveness of the proposed assistive strategy on muscle activity.

A. Participants

Two separate groups of subjects volunteered to participate in sessions #1 and #2: 10 subjects were recruited for Session #1 (10 males, age: 27.7 ± 3.5 years, height: 180.7 ± 6.9 cm, weight: 73.7 ± 10.7 kg), while 6 subjects were recruited for Session #2 (6 males, age: 29.1 ± 4.1 years, height: 178 ± 5.4 cm, weight: 70.8 ± 6.4 kg). The study was carried out at the premises of The BioRobotics Institute of Scuola Superiore Sant'Anna (Italy). The procedures were approved by the Institutional Review Board (approval n. 2/2019), and experimental activities were conducted following the principles stated in the Declaration of Helsinki. All participants signed written informed consent.

B. Experimental Setup

The setup consisted of a vertical stand with adjustable-height shelves for simulating different activities. The setup also included a screen to give instructions to the subjects and pace their movements. The setup and the tools used in the experimental tasks are shown in Fig. 3(a) and Fig. 3(b).

Six manual work tasks were simulated, with different levels of static and dynamic components [Fig. 3(c)]. *Task A* and *Task B* were defined as *box-handling tasks*: subjects were asked to move a 1-kg box from a shelf positioned at the subject's waist height to a shelf placed at head level, at two speeds, namely fast speed for *Task A*, and slow speed for *Task B*. *Task C* and *Task D* represent dynamic tasks at high shoulder angle. *Task C* was defined as a *full RoM lifting/lowering task* and consisted in lifting the box from a shelf at the subject's waist height to the overhead shelf and vice versa at self-selected speed. In *Task D*, defined as *overhead wall painting*, subjects were asked to simulate painting a vertical surface placed overhead using a roller brush. *Task E* and *Task F* represent static tasks at high shoulder angles. In *Task E*, defined as *overhead cable*

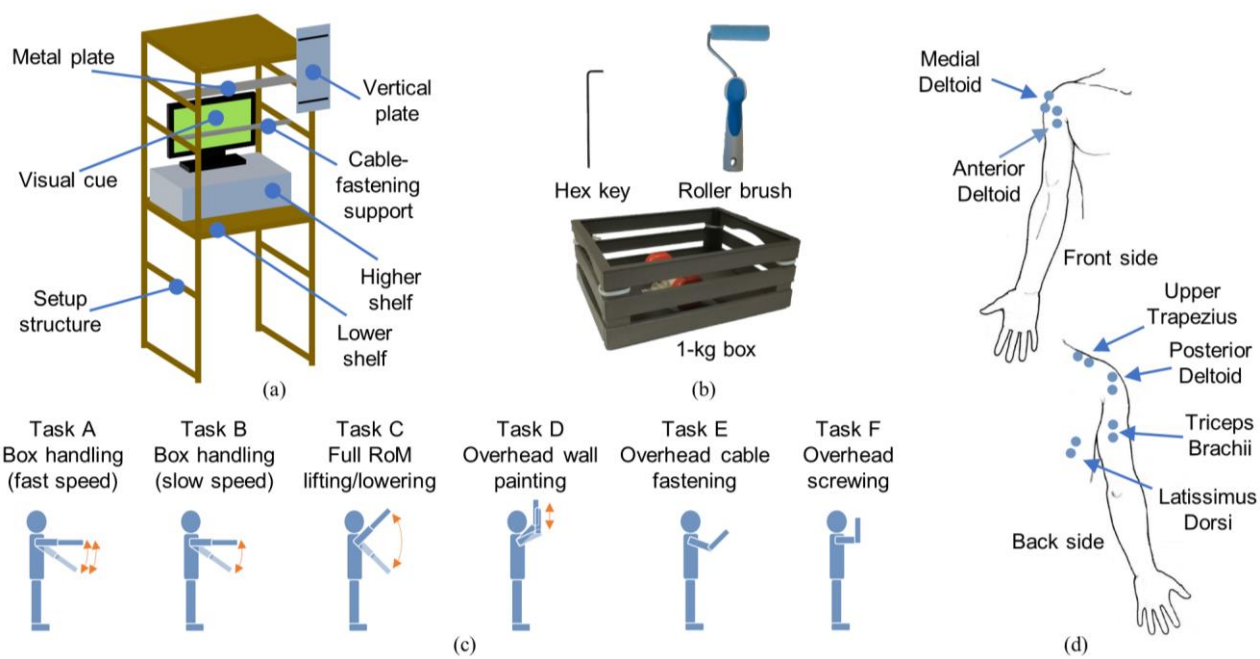

Fig. 3 (a) Experimental setup. (b) Tools used in the experimental tasks. (c) Experimental tasks. Task A to F were tested during Session #1, while Tasks B, D, and F were also tested in Session #2. (d) Schematic representation of EMG electrodes placement.

fastening, subjects were asked to continuously tighten and loosen a cable tie around the dedicated support. *Task F* was defined as *overhead screwing* and consisted of continuous fastening/unfastening of a screw inserted in the metal plate placed overhead; to perform it, subjects were requested to keep 90 deg of shoulder and elbow joints flexion.

C. Session #1: Algorithm's Output Characterization

This session aimed at characterizing the output of the algorithm across the six tasks.

Upon arrival, participants received information about the study and signed the informed consent. Then, subjects wore the exoskeleton helped by one experimenter.

Each subject tested six dyads. Each dyad consisted of two consecutive 90-seconds tasks, picked by a pseudo-random algorithm so that, overall, each task was repeated twenty times. Before starting each dyad, subjects were asked to stand still in front of the setup structure, while keeping their arms lying parallel to the body. The experimenter verbally instructed the subjects on when to start, change, and stop the tasks. A visual cue, shown through the computer screen placed in front of the subject, was also used for this purpose.

In this session, the exoskeleton output the minimum level of assistance, and sFE angular data was collected for offline analysis. This session lasted about 30 minutes.

D. Session #2: Effectiveness Assessment

This session aimed at evaluating the effectiveness of the adaptive algorithm compared to fixed assistance. The effectiveness was quantified by electromyographic measurements on three tasks, namely tasks B, D, and F, representing tasks with different levels of dynamic and static contributions.

EMG signals were collected using pre-gelled bipolar Ag/AgCl surface electrodes (Pirrone & Co., Milan, Italy) and acquired by means of the BTS FREEEMG 1000 (BTS Bioengineering, Milan, Italy). EMG signals were sampled at 1 kHz and stored locally on a laptop for offline analysis.

Upon arrival, participants received information about the study and signed the informed consent. Then, surface EMG electrodes were unilaterally applied on right-side muscles according to SENIAM guidelines [20] over the Anterior Deltoid (AD), Medial Deltoid (MD), Posterior Deltoid (PD), Upper Trapezius (UT), Triceps Brachii (TB), and Latissimus Dorsi (LD) [Fig. 3(d)].

Before starting the experiment, subjects wore the exoskeleton helped by one experimenter. A 15-minute warm-up phase allowed participants to familiarize themselves with the experimental tasks and the exoskeleton. In this phase, subjects performed several screwing/unscrewing, box handling, and painting actions while wearing the exoskeleton.

Once the warm-up phase was completed, subjects were asked to perform each task in three conditions, namely without wearing the exoskeleton (NO EXO condition), wearing the exoskeleton set to output a fixed level of assistance to compensate for about 50% of the gravitational torque on the arm (EXO-Fixed condition), and wearing the exoskeleton set to output adaptive assistance (EXO-Adaptive condition), for a total of nine experimental trials. Before each trial, subjects were asked to stand still in front of the setup with the arms lying parallel to the body, and then begin the execution of the task following the verbal instructions given by the experimenter. Each trial lasted 2 minutes. In this session, to allow intra- and inter-subjects comparison, movements of *Task B* were paced at 20 actions/min by a visual cue displayed on a computer screen in front of the subject, while movements of *Task D* were paced through a metronome at 40 actions/min. Subjects were instructed to rest between consecutive trials.

The order of the experimental conditions was randomized to avoid order effects. Within each tested condition, the order of tasks was randomized and kept identical for all three conditions. This session lasted about 2 hours.

E. Data Analysis

Data analysis was performed using custom MATLAB R2019b (The MathWorks, Natick, MA, USA) routines.

Session #1. Recorded sFE angles were used to offline compute the output of the adaptive algorithm. For each trial, for each repetition of the movement, the median value of the algorithm's output (A_{k+1}) was computed; then, the median value and interquartile range were obtained for each task.

Session #2. EMG signals were processed offline to compute the linear envelope (EMG_{Env}) by band-pass filtering (4th order Butterworth filter, cut-off frequencies: 20-400 Hz), notch filtering (4th order Butterworth filter, cut-off frequency: 50 Hz), rectifying, and low-pass filtering (zero-lag 100-ms moving average filter), before calculating outcome metrics.

For the box handling task at slow speed (*Task B)*, the last 15 actions were manually segmented into cycles by visually inspecting the total EMG (EMG_T) signal to identify onset/offset of each action. EMG_T was calculated as Eq. (4):

$$EMG_T(t) = \sum_{m=1}^{6} EMG_{Env_m}(t) \tag{4}$$

where t is the tth sample and m is the mth muscle. Then, segmented EMG signals were time normalized between 0 and 100% (EMG_{norm}) and for each muscle the integrated EMG ($IEMG$) over each cycle was computed (5):

$$IEMG_{m,n} = \int_0^{100} EMG_{norm_m}(T)\, dT \tag{5}$$

where m is the mth muscle, n is the nth cycle, and T is the Tth sample. For each subject and each muscle, the median percentage variation ($\Delta IEMG$) was computed according to the following formula (6):

$$\Delta IEMG = \left(\frac{IEMG_{avg}^{EXO} - IEMG_{avg}^{NO\ EXO}}{IEMG_{avg}^{NO\ EXO}} \cdot 100 \right) \tag{6}$$

where $IEMG_{avg}^{EXO}$ is the median $IEMG$ amplitude computed for one of the two EXO conditions (EXO-Fixed or EXO-Adaptive) and $IEMG_{avg}^{NO\ EXO}$ is the median $IEMG$ amplitude value computed for the NO EXO condition.

For the overhead wall painting and screwing tasks (*Task D* and *Task F*, respectively), the root mean square (RMS) of the EMG amplitude was obtained from the last 30 seconds of each trial.

For each subject, the median percentage variation between EXO and NO EXO conditions (ΔRMS) was calculated according to the following formula (7):

$$\Delta RMS = \left(\frac{RMS_{avg}^{EXO} - RMS_{avg}^{NO\ EXO}}{RMS_{avg}^{NO\ EXO}} \cdot 100 \right) \qquad (7)$$

Where RMS_{avg}^{EXO} is the median RMS amplitude computed for one of the two EXO conditions (EXO-Fixed or EXO-Adaptive) and $RMS_{avg}^{NO\ EXO}$ is the median RMS amplitude value computed for the NO EXO condition.

For all EMG indices, aggregated results were computed as between-subjects medians and interquartile ranges of the EMG variations between the EXO and NO EXO conditions.

F. Statistics

In Session #2, statistical analysis was conducted to assess the effect of the assistive condition (NO EXO, EXO-Fixed, EXO-Adaptive) on EMG indices.

Data violated the normality assumption, as verified by the Lilliefors test, therefore non-parametric one-way repeated-measures analysis of variance (Friedman test) was applied to check for across-conditions differences. Then, the Wilcoxon signed-rank test was used for post-hoc paired comparisons. All statistical analyses were performed in MATLAB R2019b using a significance level $\alpha < 5\%$.

V. Results

A. Session #1: Algorithm's Output Characterization

The average output of the algorithm is shown in Fig. 4. In tasks *A*, *B*, *C* the algorithm output the minimum assistance level (i.e., close to level 0), while for tasks *D*, *E*, *F* the output of the algorithm resulted close to 1, 5, and 6, respectively.

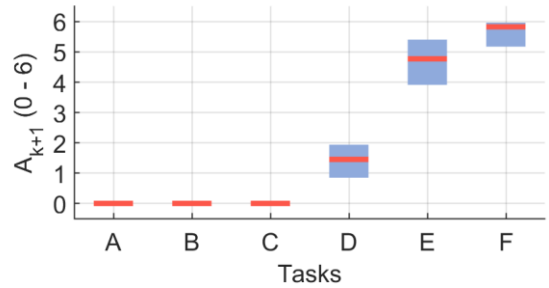

Fig. 4 Algorithm's output for the six experimental tasks, expressed as median values and interquartile ranges. A: box handling at fast speed; B: box handling at slow speed; C: full RoM lifting/lowering; D: overhead wall painting; E: overhead cable fastening; F: overhead screwing.

B. Session #2: Algorithm Effectiveness

Fig. 5 shows the results of the EMG analysis for the three tasks B, D, and F.

In *Task B*, when using the exoskeleton, the $IEMG$ of the AD, MD, UT, and TB muscles significantly reduced compared to the NO EXO condition, regardless of the assistive strategy ($\chi^2(2) = 10.3$, $p = 0.006$ for AD and MD; $\chi^2(2) = 6.3$, $p = 0.042$ for UT; $\chi^2(2) = 9.3$, $p = 0.009$ for TB). Significant differences between fixed and adaptive assistance were found for the MD muscle ($p = 0.031$).

In *Task D*, all muscles exhibited reduced EMG RMS values when using the exoskeleton with respect to the NO EXO condition ($\chi^2(2) = 10.3$, $p = 0.006$ for AD, MD, PD; $\chi^2(2) =$

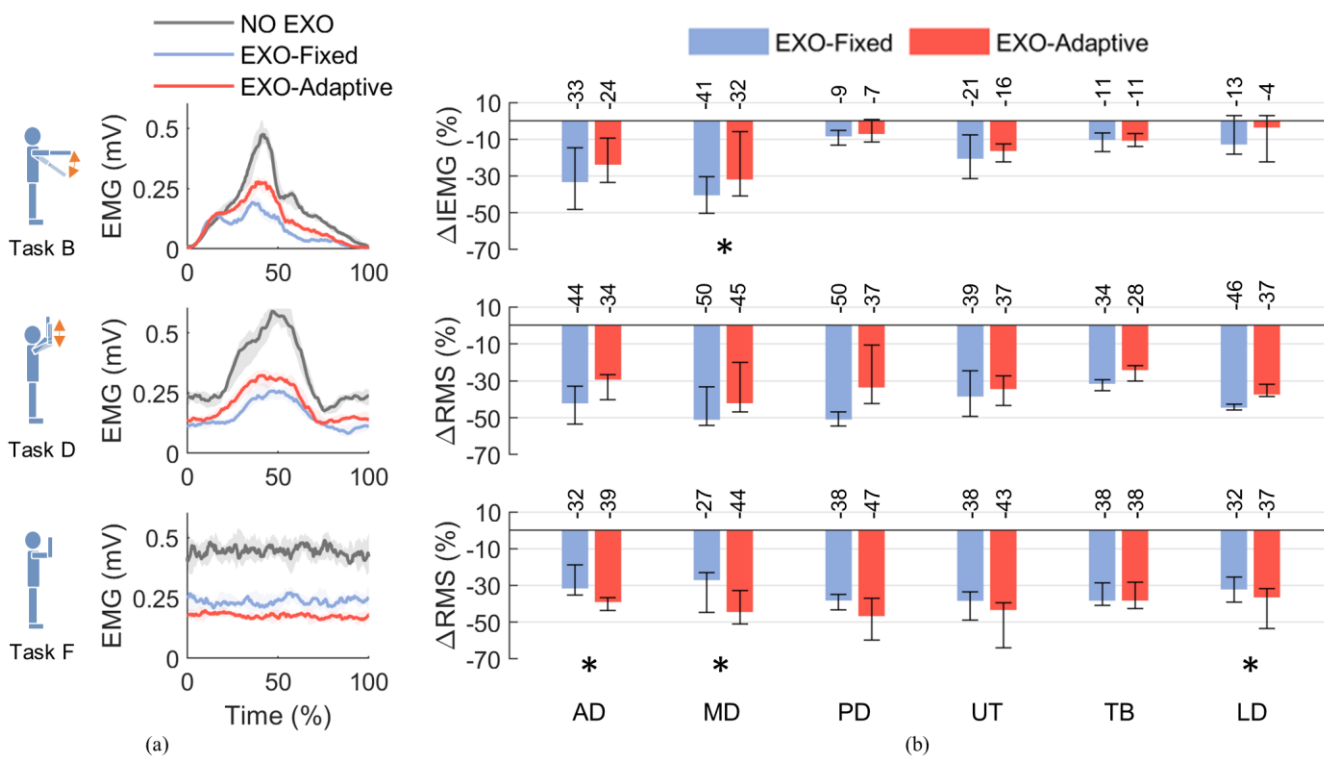

Fig. 5 (a) Example of EMG profiles for the Anterior Deltoid of a representative subject. (b) EMG results are shown for Anterior Deltoid (AD), Medial Deltoid (MD), Posterior Deltoid (PD), Upper Trapezius (UT), Triceps Brachii (TB), and Latissimus Dorsi (LD). Bars represent percentage variations of the RMS and IEMG indices, with respect to NO EXO. Results are reported for box-handling, overhead wall painting, and overhead screwing tasks. The EXO-Fixed condition corresponded to about 5.4 Nm, while the EXO-Adaptive condition corresponded to about 4.5, 4.7, and 6 Nm for Task B, D, and F, respectively. Asterisks mark statistically significant differences between EXO conditions. Median percentage variations are shown over each bar.

9.3, p = 0.009 for UT, TB, LD). No significant differences between EXO conditions were found, although AD, MD, and PD variations were close to significance (p = 0.062).

In *Task F*, all muscles showed decreased EMG RMS in EXO conditions compared to the NO EXO condition ($\chi^2(2)$ = 12, p = 0.003 for AD, MD, LD; $\chi^2(2)$ = 10.3, p = 0.006 for PD, UT; $\chi^2(2)$ = 9, p = 0.011 for TB). Significantly different values were also found in AD, MD, and LD muscles between the two EXO conditions (p = 0.031 for all pairwise comparisons).

VI. Discussion

In this article, we presented a novel algorithm that aims to tune the assistance level of a spring-loaded semi-passive upper-limb exoskeleton according to the kinematics characteristics of the task. In particular, the algorithm was designed to output higher assistance in static tasks performed with arms elevated (around 90 deg), with the aim to support the action of the flexor and abductor muscles that are mostly involved in maintaining the arms posture by counterbalancing the arm's gravitational load, and to output lower assistance in dynamic tasks, in order to limit the need for the extensor muscles to contract to lower the arms while still supporting the flexors' eccentric work in this phase.

As shown in the results of Session #1, the three most dynamic tasks (tasks *A*, *B*, and *C*), resulted in minimum assistance, whereas the algorithm generated three different outputs for the three overhead tasks, namely tasks *D*, *E*, and *F*, with assistance levels 1, 5 and 6, respectively. Overall, these outputs were in line with our initial design assumptions, with the maximum assistance level provided in the overhead static screwing task (*Task F*), slightly lower assistance levels in the cable-fastening task (*Task E*) due to a lower shoulder elevation, and even lower assistance for the wall painting task (*Task D*) due to high dynamicity of the task. These results were consistent for all subjects showing robustness to the user's anthropometric sizes (i.e., height and weight). Also, the output of the algorithm was always identical for the right and left arms as the tasks were bimanual and symmetrical but in the case of asymmetric tasks, the assistance level could be different for the two arms.

In Session #2, the effect of the adaptive assistance was evaluated against the condition in which the exoskeleton was not worn (NO EXO) and against the condition of a fixed level of assistance (EXO-Fixed). The fixed level was determined to compensate for about 50% of the gravitational torque on the shoulder, similar to the fraction typically relieved by passive exoskeletons [13]; in this experiment, it corresponded to assistance level 4 for all subjects, whereas the adaptive level corresponded to 0, 1, and 6 for tasks *B*, *D*, and *F*, respectively.

Overall, for almost all muscles and in all tasks, the use of the exoskeleton reduced muscles' physical strain compared to the NO EXO condition; however, the comparison of the two assistance strategies showed differences in the three tasks.

In the dynamic box handling task, the EXO-Fixed condition led to higher reductions than the EXO-Adaptive for AD and MD muscles. Indeed, for agonist muscles the smaller assistive torque delivered according to the adaptive strategy (i.e., the minimum one) appeared to be less effective. This effect might be explained considering that agonist muscles exert the maximum power in the lifting phase of the movement (i.e., moving the box from the lower to the upper shelf), thus taking advantage of the higher torque, as suggested in [21]. Therefore, there was no significant difference between the two assistances when looking at antagonist muscles. This seems to be in contrast with other studies, where higher support levels lead to higher muscle effort [19], [22]. One of our goals was the attempt to reduce the hindrance caused by the exoskeleton's springs in highly dynamic movements. However, our findings could suggest that this hindering effect is negligible when dynamic movements are performed in favor of gravity (i.e., when moving the box from the higher to the lower shelf).

In the overhead wall-painting, similarly to the box handling case, the EXO-Fixed condition ensured a greater assistance level than the EXO-Adaptive one (i.e., 4 vs. 1 on average) and higher assistance was again associated with greater EMG reductions. This task is particularly interesting because the subjects needed to perform wide and fast movements around an average angle of around 90 deg. Hence, again, the greater assistance did not lead to side effects on the shoulder extensor muscles, despite the dynamic nature of the task.

In the screwing task, regardless of the experimental conditions, all monitored muscles showed significantly smaller activations in both shoulder flexion agonists (AD, MD, UT) and antagonists (PD, TB, LD) with the exoskeleton. Coherently with our previous study [15] and other similar works [18], [22], a higher level of assistance led to increased EMG reductions while performing the static overhead task, especially for shoulder flexion agonists, as these muscles need to generate less force to maintain the posture as the gravitational support increases [8]. This led to a reduced co-contraction of the antagonist muscles that are used to stabilize the shoulder [9].

Results on EMG data suggest that not all the assumptions made in the design phase of the algorithm were effective. Indeed, the adaptive assistance led to higher EMG reductions in the static task with respect to the fixed assistance, but the same behavior was not observed in the more dynamic tasks, in which the fixed assistance showed higher effectiveness than the adaptive one. In other words, in both static and dynamic tasks higher EMG reductions were achieved with higher assistance levels, and in no cases, did the assistance cause detrimental effects on the antagonist muscles. Notably, due to the limited torque range of the exoskeleton, in all conditions, the torque exerted by the exoskeleton was only a portion of the arms' gravitational torque (between about 40 to 60%). In dynamic tasks, this means that in both conditions (EXO-Fixed and EXO-Adaptive) the net gravitational torque at the shoulders was always sufficient to perform extension movements without causing overexertion (i.e., concentric contraction) of the antagonist muscles. Hence, in dynamic tasks, high percentages of antigravitational support (close to or higher than the user's arm gravitational torque) would have likely resulted in detrimental effects on the antagonist muscles [18], whereas in static tasks assistance levels close to 100% of the gravitational torque may have led to even further EMG reductions [15], [18]. Also, the small torque range could have limited the observation of large EMG differences between the

EXO conditions. The results suggest possible improvements to the adaptive algorithm, which in addition to considering the kinematic characteristics of the task, should also be tailored to the user's anthropometry by including the desired percentage of arm's antigravitational support in the equations.

A. Limitations of the Study and Future Works

While the results of electromyographic activity should be considered as the first proof of the efficacy of the proposed algorithm, the exploratory nature of the tests did not permit to investigate some important factors that could influence EMG results. Among all, the duration of the trials or the experience of the subjects with the technology could have a significant impact on the EMG reductions and further enhance the effects of the exoskeleton in real-use conditions. In particular, as task duration is directly correlated to the increase in muscle fatigue and muscle activation, it is possible to hypothesize that the assistance of the exoskeleton could delay the occurrence of fatigue and lead to even higher reductions in the muscle activation over time compared to the NO EXO condition [23], [24]. Also, several studies have suggested how longer familiarization sessions with an exoskeleton can maximize the effectiveness of human-robot cooperation [11], [18], [19], [25].

Also, in its current implementation, the adaptive algorithm is highly dependent on the features' values computed in the previous time window, which can cause sudden variations in the A_{k+1} value, although these abrupt changes are filtered out by the slow dynamics of the actuator and by the implementation of software controls. Additionally, the algorithm does not take into account external load conditions, thus reducing its ability to adapt to the use of working tools of different weights.

Finally, due to the preliminary evaluation of the algorithm on inexperienced young subjects, the algorithm has not been assessed in terms of perceived efficacy or usefulness, which could be evaluated in future tests with experienced workers.

Future works will focus on refining the algorithm and testing with a wider pool of subjects in more realistic environments, namely in real work tasks and in longer trials, where also the effects of fatigue might be assessed.

REFERENCES

[1] H. T. Leong, S. C. Fu, X. He, J. H. Oh, N. Yamamoto, and S. H. P. Yung, "Risk factors for rotator cuff tendinopathy: A systematic review and meta-analysis," *J. Rehabil. Med.*, vol. 51, no. 9, pp. 627–637, 2019, doi: 10.2340/16501977-2598.

[2] T. Butler and J. C. Gillette, "Exoskeletons: Used as PPE for Injury Prevention," *Prof. Saf. J.*, pp. 32–37, 2019.

[3] S. Crea *et al.*, "Occupational exoskeletons: A roadmap toward large-scale adoption. Methodology and challenges of bringing exoskeletons to workplaces," *Wearable Technol.*, vol. 2, 2021, doi: 10.1017/wtc.2021.11.

[4] S. De Bock *et al.*, "Benchmarking occupational exoskeletons: An evidence mapping systematic review," *Appl. Ergon.*, vol. 98, no. September 2021, 2022, doi: 10.1016/j.apergo.2021.103582.

[5] B. Otten, R. Weidner, and A. Argubi-Wollesen, "Evaluation of a novel active exoskeleton for tasks at or above head level," *IEEE Robot. Autom. Lett.*, vol. 3, no. 3, pp. 1–1, 2018, doi: 10.1109/LRA.2018.2812905.

[6] Y. M. Zhou, C. Hohimer, T. Proietti, C. T. O'Neill, and C. J. Walsh, "Kinematics-Based Control of an Inflatable Soft Wearable Robot for Assisting the Shoulder of Industrial Workers," *IEEE Robot. Autom. Lett.*, vol. 6, no. 2, pp. 2155–2162, 2021, doi: 10.1109/LRA.2021.3061365.

[7] P. Maurice *et al.*, "Objective and Subjective Effects of a Passive Exoskeleton on Overhead Work," *IEEE Trans. Neural Syst. Rehabil. Eng.*, p. 1, 2019, doi: 10.1109/TNSRE.2019.2945368.

[8] T. Schmalz *et al.*, "Biomechanical and metabolic effectiveness of an industrial exoskeleton for overhead work," *Int. J. Environ. Res. Public Health*, vol. 16, no. 23, 2019, doi: 10.3390/ijerph16234792.

[9] I. Pacifico *et al.*, "An Experimental Evaluation of the Proto-MATE: A Novel Ergonomic Upper-Limb Exoskeleton to Reduce Workers' Physical Strain," 2020, doi: 10.1109/MRA.2019.2954105.

[10] S. De Bock *et al.*, "Passive Shoulder Exoskeletons: More Effective in the Lab than in the Field?," *IEEE Trans. Neural Syst. Rehabil. Eng.*, vol. 29, no. 2016, pp. 173–183, 2020, doi: 10.1109/TNSRE.2020.3041906.

[11] I. Pacifico *et al.*, "Exoskeletons for workers: A case series study in an enclosures production line," *Appl. Ergon.*, vol. 101, no. January, p. 103679, 2022, doi: 10.1016/j.apergo.2022.103679.

[12] I. Pacifico *et al.*, "Using a Spring-Loaded Upper-Limb Exoskeleton in Cleaning Tasks: A Preliminary Study BT - Wearable Robotics: Challenges and Trends," 2022, pp. 481–485.

[13] M. Rossini *et al.*, "Design and performance evaluation of a wearable passive cable-driven shoulder exoskeleton," *IEEE Trans. Med. Robot. Bionics*, 2021, doi: 10.1109/TMRB.2021.3110679.

[14] F. Missiroli *et al.*, "Rigid, Soft, Passive, and Active: a Hybrid Occupational Exoskeleton for bimanual multijoint assistance," *IEEE Robot. Autom. Lett.*, vol. 7, no. 2, pp. 2557–2564, 2022, doi: 10.1109/LRA.2022.3142447.

[15] L. Grazi, E. Trigili, G. Proface, F. Giovacchini, S. Crea, and N. Vitiello, "Design and experimental evaluation of a semi-passive upper-limb exoskeleton for workers with motorized tuning of assistance," *IEEE Trans. Neural Syst. Rehabil. Eng.*, no. c, pp. 1–1, 2020, doi: 10.1109/tnsre.2020.3014408.

[16] F. Giovacchini, M. Moisè, G. Proface, L. Morelli, and N. Vitiello, "System for assisting an operator in exerting efforts," WO2020217191A1, 2020.

[17] D. L. Bartel, D. T. Davy, and T. Keaveny, *Orthopaedic biomechanics: mechanics and design in musculoskeletal systems*. Prentice Hall, 2006.

[18] L. Van Engelhoven, N. Poon, H. Kazerooni, D. Rempel, A. Barr, and C. Harris-Adamson, "Experimental Evaluation of a Shoulder-Support Exoskeleton for Overhead Work: Influences of Peak Torque Amplitude, Task, and Tool Mass," *IISE Trans. Occup. Ergon. Hum. Factors*, vol. 7, no. 3–4, pp. 250–263, 2019, doi: 10.1080/24725838.2019.1637799.

[19] J. Theurel, K. Desbrosses, T. Roux, and A. Savescu, "Physiological consequences of using an upper limb exoskeleton during manual handling tasks," *Appl. Ergon.*, vol. 67, pp. 211–217, 2018, doi: https://doi.org/10.1016/j.apergo.2017.10.008.

[20] H. J. Hermens, B. Freriks, C. Disselhorst-Klug, and G. Rau, "Development of recommendations for SEMG sensors and sensor placement procedures," *J. Electromyogr. Kinesiol.*, vol. 10, no. 5, pp. 361–374, 2000.

[21] K. Huysamen, V. Power, and L. O'Sullivan, "Kinematic and kinetic functional requirements for industrial exoskeletons for lifting tasks and overhead lifting," *Ergonomics*, vol. 63, no. 7, pp. 818–830, 2020, doi: 10.1080/00140139.2020.1759698.

[22] L. Van Engelhoven, N. Poon, H. Kazerooni, A. Barr, D. Rempel, and C. Harris-Adamson, "Evaluation of an adjustable support shoulder exoskeleton on static and dynamic overhead tasks," in *Proceedings of the Human Factors and Ergonomics Society Annual Meeting*, 2018, vol. 62, no. 1, pp. 804–808, doi: 10.1177/1541931218621184.

[23] C. A. Lotz, M. J. Agnew, A. A. Godwin, and J. M. Stevenson, "The effect of an on-body personal lift assist device ({PLAD}) on fatigue during a repetitive lifting task," *J. Electromyogr. Kinesiol.*, vol. 19, no. 2, pp. 331–340, Apr. 2009, doi: 10.1016/j.jelekin.2007.08.006.

[24] P. Yin, L. Yang, S. Qu, and C. Wang, "Effects of a passive upper extremity exoskeleton for overhead tasks," *J. Electromyogr. Kinesiol.*, vol. 55, no. January, p. 102478, 2020, doi: 10.1016/j.jelekin.2020.102478.

[25] S. Alabdulkarim and M. A. Nussbaum, "Influences of different exoskeleton designs and tool mass on physical demands and performance in a simulated overhead drilling task," *Appl. Ergon.*, vol. 74, pp. 55–66, 2019, doi: https://doi.org/10.1016/j.apergo.2018.08.004.